doi:10.2533/chimia.2015.220 Chimia 69 (2015) 220–224

$WO_3/CeO_2/TiO_2$ Catalysts for Selective Catalytic Reduction of NO_x by NH_3: Effect of the Synthesis Method

Katarzyna A. Michalow-Mauke§*[a], Ye Lu[b], Davide Ferri[a], Thomas Graule[c], Kazimierz Kowalski[d], Martin Elsener[a], and Oliver Kröcher*[ae]

§SCS-DSM Award for best poster presentation

Abstract: $WO_3/CeO_2/TiO_2$, CeO_2/TiO_2 and WO_3/TiO_2 catalysts were prepared by wet impregnation. CeO_2/TiO_2 and WO_3/TiO_2 showed activity towards the selective catalytic reduction (SCR) of NO_x by NH_3, which was significantly improved by subsequent impregnation of CeO_2/TiO_2 with WO_3. Catalytic performance, NH_3 oxidation and NH_3 temperature programmed desorption of wet-impregnated $WO_3/CeO_2/TiO_2$ were compared to those of a flame-made counterpart. The flame-made catalyst exhibits a peculiar arrangement of W-Ce-Ti-oxides that makes it very active for NH_3-SCR. Catalysts prepared by wet impregnation with the aim to mimic the structure of the flame-made catalyst were not able to fully reproduce its activity. The differences in the catalytic performance between the investigated catalysts were related to their structural properties and the different interaction of the catalyst components.

Keywords: Flame spray synthesis · NH_3 · NO_x reduction · SCR · Wet impregnation

Introduction

The major source of nitrogen oxides (NO_x) emissions is the combustion of fossil fuels in vehicle engines and power plants. NO_x are formed thermally in the combustion process from N_2 and O_2 present in the supplied air. They are a major source of air pollution causing the formation of ozone, photochemical smog and acid rain.[1] NO_x emissions from lean burn diesel engines are efficiently treated by the selective catalytic reduction using ammonia (NH_3-SCR) (Eqn. (1)).[2,3]

Standard SCR
$$4NO + 4NH_3 + O_2 \rightarrow 4N_2 + 6H_2O \quad (1)$$

Catalysts based on V_2O_5–WO_3/TiO_2 are most widely used in automotive and stationary applications. However, this very efficient catalytic system suffers from several drawbacks. Low thermal and hydrothermal stability with the resulting catalyst deactivation and simultaneous release of tungsten and vanadium species to the environment are the most detrimental. Therefore, there is an urgent demand to develop new thermally stable catalysts, which should also be cost-effective. In recent years, CeO_2 has received considerable attention in three-way catalysis due to its oxygen storage capacity and the high redox ability of the Ce^{4+}/Ce^{3+} pair, which make it attractive also for use in SCR catalysts.[4] CeO_2 possesses some intrinsic SCR activity,[5] but its performance improves significantly when it is functionalized by another transition metal oxide. CeO_2-TiO_2 and CeO_2-WO_3-TiO_2 catalysts synthesized by various techniques, *e.g.* wet impregnation (WI),[6] sol-gel (SG),[7] co-precipitation (CP)[8] or flame spray synthesis (FSS),[9] displayed remarkable SCR activity. Recently, we have shown that understanding of the catalyst structure and the interaction of the catalyst components is crucial for the optimization of its performance.[9b] Flame-made $WO_3/CeO_2/TiO_2$ nanomaterials demonstrated excellent activity for the selective catalytic reduction of NO_x by NH_3. The highest activity was observed for 10 wt% WO_3/10 mol% CeO_x-90 mol% TiO_2, which was comparable to a benchmark V-W/Ti catalyst. This exceptional catalytic performance was related to its peculiar structure (Fig. 1) where CeO_2 protrusions on TiO_2 particles are homogenously covered by amorphous WO_3. The arrangement of the metal oxide phases on TiO_2 is opposite to that commonly applied in conventional synthesis procedures. Moreover, we have shown that TiO_2 is not only a support material but its close interaction with CeO_2 is crucial to induce high surface concentration of Ce^{3+}, which is considered an SCR active site. The presence of a layer of amorphous WO_3 on the surface of the entire catalyst provided an appropriate surface acidity for NH_3 adsorption and significantly improved N_2 selectivity. Therefore, the arrangement and

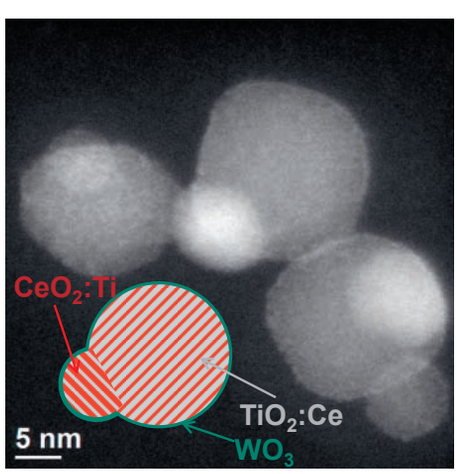

Fig. 1. STEM image of FSS-W/Ce/Ti with schematic illustration of the material composition.

*Correspondence: Dr. K. A. Michalow-Mauke[a], Dr. O. Kröcher[ae]
E-mail k.michalow.mauke@outlook.com, oliver.kroecher@psi.ch
[a]Paul Scherrer Institute, CH-5232 Villigen
[b]Lab. for Solid State Chemistry and Catalysis
[c]Lab. for High Performance Ceramics
Empa Swiss Federal Laboratories for Materials Science and Technology
Überlandstrasse 129, CH-8600 Dübendorf
[d]Faculty of Metals Engineering & Industrial Computer Science
AGH University of Science & Technology
Al. Mickiewicza 30, PL-30059 Krakow, Poland
[e]Institute of Chemical Sciences and Engineering
EPF Lausanne

the interaction between each component in the catalyst are essential for its activity.

In this work, we tried to mimic the peculiar composite-like structure of the catalyst obtained by flame spray synthesis using conventional wet impregnation, which is cheaper and widely used. For this purpose we replicated the flame-spray catalyst by depositing CeO_2 on TiO_2 followed by impregnation with the tungsten precursor. The main purpose of this study was to unravel the effect of the arrangement of WO_3 on the catalyst activity.

Experimental

Synthesis

The SCR catalysts, with the compositions listed in Table 1, were prepared by wet impregnation (WI) and flame spray synthesis (FSS). Commercially available TiO_2 (DT51, Crystal Global) was suspended in water by ultrasonication; then, an aqueous solution of cerium (III) nitrate ($Ce(NO_3)_3 \cdot 6H_2O$, assay ≥ 99%, Fluka) or ammonium metatungstate ($(NH_4)_{10}(H_2W_{12}O_{42} \cdot 4H_2O$, assay 85%, Aldrich) was added to obtain 10 mol% Ce/90 mol% TiO_2 and 10 wt% WO_3/TiO_2, respectively. After 10 min of ultrasonication, mixing in the rotavapor for 1 h and drying in vacuum at 70˚C, the powders were further dried in the oven at 120˚C for 12 h and calcined at 550˚C for 5 h. The 10 mol% Ce/90 mol% TiO_2 powder was ball milled (600 rpm, 2 min) with the addition of water and further impregnated with ammonium metatungstate ($(NH_4)_{10}(H_2W_{12}O_{42} \cdot 4H_2O$, assay 85%, Aldrich) to obtain 10 wt% WO_3/10 mol% Ce/90 mol% TiO_2.

In the case of flame-spray synthesis, titanium diisopropoxide bis(acetylacetonate) ($TiC_{16}H_{28}O$, 75% in isopropanol, ABCR), cerium (III) ethylhexanoate ($Ce[OOCCH(C_2H_5)C_4H_9]_3$, Ce content: 11.8-12.2%, Shepherd) and tungsten carbonyl ($W(CO)_6$, Sigma-Aldrich) precursors were dissolved in tetrahydrofurane (Sigma-Aldrich). Details of the flame spray setup are reported elsewhere.[10] The required composition of the produced particles was obtained by adjusting the ratios of the different precursors in the precursor mixture. The total precursor concentration in the flame was kept constant at 0.5 mol·kg^{-1}. The precursor solution was fed by a syringe pump and was atomized by oxygen in a gas-assisted external mixing nozzle. The combustible aerosol was ignited by six acetylene-oxygen flamelets (C_2H_2, 217 cm^3·s^{-1}; O_2, 283 cm^3·s^{-1}) and the produced particles were collected on glass fiber filters (GF/A 150, Whatman) using vacuum pumps.

Structural Characterization

The specific surface area (SSA) was determined using a Quantachrome Autosorb 1C instrument from the N_2 adsorption/desorption isotherm using the Brunauer-Emmett-Teller (BET) method. Prior to analysis, powder samples were dried for 120 min at 180˚C in N_2.

X-ray diffraction (XRD) patterns were collected in the range of 5˚<2θ<80˚ using a Bruker D8 Advance diffractometer equipped with a Ni-filtered Cu-Kβ radiation and a LinxEye detector. The phase identification was based on inorganic crystal structure database (ICSD) data files.

Catalytic Activity

NH_3-SCR experiments were conducted in a quartz tube plug flow reactor. The catalyst (50 mg) was mixed with 0.5 g of 100–160 μm cordierite and firmly fixed between two quartz wool plugs. A thermocouple was inserted at the front end of the catalyst bed. The sample was pre-treated with 10 vol% O_2 in N_2 supplied at 450 ˚C for 45 min. The model gas feed for the activity test was composed of 10 vol% O_2, 5 vol% H_2O, 1000 ppm NO, 1200 ppm NH_3 (N_2 bal.). For NH_3 oxidation experiments, the feed gas consisted of 1000 ppm NH_3 10 vol% O_2, 5 vol% H_2O (N_2 bal.). For all experiments, the gas flow rate was 100 mL·min^{-1} (GHSV = 120 L·g^{-1}·h^{-1}). The reactor effluent was monitored online by FTIR spectroscopy (Thermo Scientific Antaris). The NO_x conversion expressed as $DeNO_x$ was calculated as follows:

$$DeNO_x = \frac{NO_{x,in} - NO_{x,out}}{NO_{x,in}} \quad (2)$$

with

$$NO_x = C_{NO_2} + C_{NO} + 2 \cdot C_{N_2O} \quad (3)$$

Temperature Programmed Desorption

NH_3 temperature programmed desorption (NH_3-TPD) was applied to assess the surface acidity of the catalysts and their NH_3 uptake (normalized by mass and specific surface area of the material). NH_3-TPD was performed in the same quartz tube plug flow reactor used for the catalytic tests. Prior to TPD, the sample was pre-treated with 10 vol% O_2 in N_2 at 500 ˚C for 1h and then cooled to 50 ˚C in N_2. NH_3 (1000 ppm in N_2) was supplied for adsorption for 1 h at 50 ˚C. The physisorbed species were removed by flowing N_2 at 50 ˚C for 1 h. The NH_3-TPD were carried out under N_2 flow from 50 to 500 ˚C at 10 ˚C·min^{-1}. The gas composition was monitored online by FTIR spectroscopy (Thermo Scientific Antaris). Deconvolution of the TPD profiles was carried out with the Fityk program for data processing and nonlinear curve fitting.[11]

Table 1. Composition, specific surface area (SSA), WO_3 coverage and NH_3 uptake of all catalysts.

Sample name	Composition	SSA / $m^2 \cdot g^{-1}$	WO_3 coverage[a] / –	NH_3 uptake / ppm m^{-2}
V-W/Ti	2.4 wt%V_2O_5-10 wt% WO_3 / TiO_2	60.5	0.95	6771
FSS_Ti	TiO_2	93.3	–	6820
FSS_W/Ti	10 wt% WO_3/ TiO_2	89.9	0.64	7047
FSS_Ce/Ti	10 mol% CeO_2/90 mol% TiO_2	95.6	–	4708
FSS_W/Ce/Ti	10 wt% WO_3/ 10 mol% CeO_2/90 mol% TiO_2	94.0	0.64	5540
WI_Ti	TiO_2 (DT51) untreated	93.1	–	21929
WI_Ti-550	TiO_2 (DT51) after 550 ˚C heat treatment	74.3	–	–
WI_W/Ti	10 wt% WO_3/ TiO_2	61.0	0.95	9092
WI_Ce/Ti	10 mol%CeO_2/90 mol% TiO_2	65.1	–	5737
WI_W/Ce/Ti	10 wt% WO_3/ 10 mol% CeO_2/90 mol% TiO_2	53.2	1.09	6436

[a]WO_3 monolayer = 4.5 W atoms·nm^{-2}[14]

Results and Discussion

$WO_3/CeO_2/TiO_2$ SCR catalysts were prepared by two different synthesis methods: wet impregnation and flame spray synthesis. Binary CeO_2/TiO_2 and WO_3/TiO_2 were also prepared in order to rationalize the effect of each component on the catalytic performance. The composition of all catalysts is listed in Table 1.

The comparison of the X-ray diffraction patterns of the catalysts (Fig. 2) shows clear structural dissimilarities that can be associated with the synthesis methods. The commercial TiO_2 support for wet-impreg-

nation (WI_Ti) consists of the metastable anatase polymorph (ICSD 01-084-1285), which retained its structure after calcination at 550 °C (Fig. 2a) despite the loss of *ca.* 20% of specific surface area (SSA, Table 1). Anatase was the only TiO_2 phase present in the WI samples. Wet impregnation of TiO_2 by WO_3, CeO_2 and by both of them followed by calcination gradually decreased the SSA but did not affect the primary structure of the support. XRD indicates that both WO_3 and CeO_2 are present in crystalline form in WI_W/Ti, WI_Ce/Ti and WI_W/Ce/Ti catalysts suggesting the clear separation of each oxide component at least at XRD level. Given the low contribution of cubic WO_3 (ICSD 00-046-1096) to the XRD of WI_W/Ti, we can assume that this phase coexists with a fraction of amorphous WO_3. On the contrary, the XRD patterns of FSS_W/Ti and FSS_W/Ce/Ti catalysts did not show any indication of crystalline WO_3 (Fig. 2b) supporting the evidence that WO_3 formed only an amorphous layer on TiO_2 and on CeO_2/TiO_2 (Fig. 1). A significant difference can also be seen between diffraction patterns of WI_Ce/Ti and FSS_Ce/Ti catalysts. In the former catalyst, cerium is present as crystalline cubic CeO_2 (ICSD 00-004-0593) and does not form phases with tungsten or titanium. The diffraction pattern of FSS_Ce/Ti is more complicated. Beside cubic CeO_2, the brannerite $CeTi_2O_6$ (ICSD 01-084-0496) structure was detected which is indicative of a defined Ce-Ti interaction. Moreover, the fraction of rutile TiO_2 (ICSD 01-087-0920), the thermally stable TiO_2 polymorph, significantly increases at the expense of anatase. The phase transformation was associated with the presence of a large fraction of Ce^{3+} observed by XPS and by its incorporation in the TiO_2 lattice.[9b] Oxygen vacancies allow structural rearrangement and promote an anatase to rutile transformation.[12] Diffraction patterns of WI_W/Ce/Ti and FSS_W/Ce/Ti appear as the simple combination of the patterns of the corresponding binary systems.

The structural differences between wet-impregnated and flame-made materials caused the observed changes of NH_3-SCR activity. Addition of WO_3 (WI_W/Ti) improved significantly the performance of bare TiO_2 (Fig. 3) with full NO_x conversion ($DeNO_x$) at 400 °C, which rapidly dropped to 13% at 300 °C. The $DeNO_x$ curve of WI_W/Ti was shifted to lower temperature compared to that of the same composition prepared by flame-spray synthesis (FSS_W/Ti). This difference could be attributed to the high coverage of mixed crystalline and amorphous WO_3 in WI_W/Ti.[13] The difference in the catalytic activity is even more pronounced for the Ce/Ti samples. The operating temperature window of FSS_Ce/Ti was extended towards low temperature, showing more than 30% $DeNO_x$ at 200 °C and nearly full conversion at 300 °C. In contrast, the $DeNO_x$ curve of WI_Ce/Ti presented a maximum of conversion of only 49% at 300 °C, the overall performance of this material being inferior to that of the flame-made counterpart. WI_Ce/Ti was also less selective and produced a significant amount of undesired N_2O, 88 ppm at 300 °C. Under the same SCR experimental conditions, FSS_Ce/Ti produced only 17 ppm of N_2O slip at 450 °C. The better dispersion of Ce-containing phases (Fig. 2) and the presence of Ce^{3+}[9b] in FSS_Ce/Ti are probably responsible for the superior performance of this material. Deposition of WO_3 on CeO_2/TiO_2 caused in both cases an enhancement of $DeNO_x$ activity and improved product selectivity. No N_2O slip was detected in WI_W/Ce/Ti and FSS_W/Ce/Ti catalysts. The promoting role of WO_3 of both WI- and FSS-made catalysts is in agreement with the literature.[4] FSS_W/Ce/Ti clearly outperformed the equivalent catalyst prepared by wet impregnation and its activity was comparable to that of 2.4 wt% V_2O_5-10 wt% WO_3/TiO_2 (V-W/Ti). Therefore, the choice of the synthesis method greatly affected the catalytic performance.

During NH_3-SCR several reactions influence the overall catalyst performance. NH_3 oxidation is an undesired reaction that decreases the efficiency of the SCR process. The propensity of all catalysts to oxidize NH_3 was tested independently from the NH_3-SCR tests (Fig. 4). The NH_3 oxidation activity of WI_Ce/Ti was remarkable over all the temperature range investigated. Contrary to FSS_Ce/Ti, WI_Ce/Ti produced larger amounts of NO_2, NO and N_2O, which we consider a consequence of the presence of well-crystallized cubic ceria (Fig. 2a). This NH_3 oxidation activity of WI_Ce/Ti explains the drop of $DeNO_x$ activity above 300 °C observed in Fig. 3. NH_3 oxidation was suppressed once WO_3 was deposited on the Ce/Ti catalyst.

The presence of WO_3 on the surface of CeO_2/TiO_2 blocked some of the oxidation active sites of CeO_2 and improved

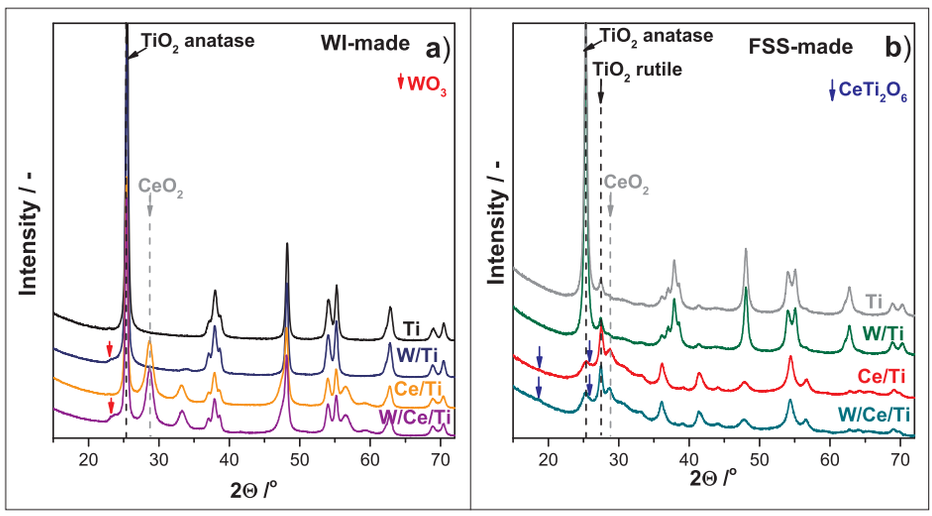

Fig. 2. X-ray powder diffraction patterns of wet-impregnated (a) and flame-made (b) catalysts.

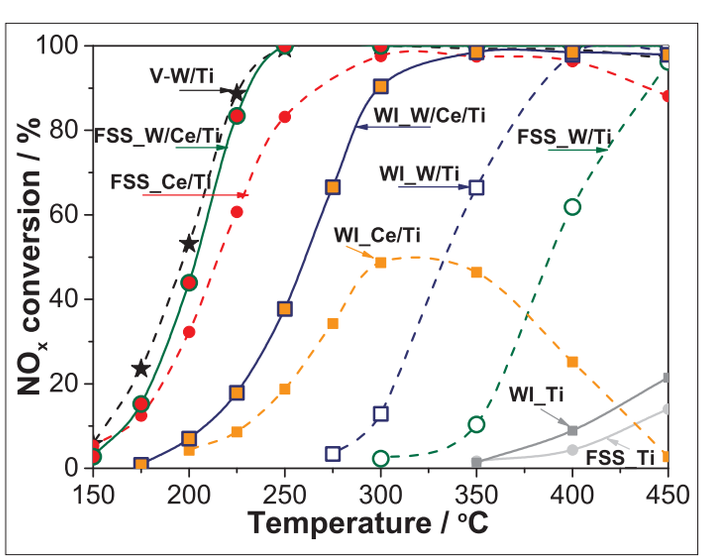

Fig. 3. NO_x conversion of all catalysts.

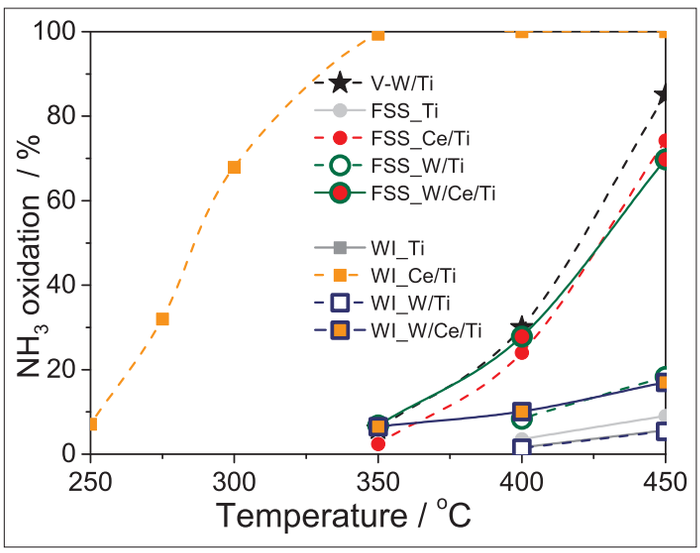

Fig. 4 NH_3 oxidation activity of all catalysts.

catalysts selectivity by conveying surface acidity, which was studied by temperature programmed desorption of NH_3 (NH_3-TPD, Fig. 5). The NH_3 uptake levels of all catalysts are reported in Table 1. Although the catalytic performance of FSS- and WI-made materials is different, they behave very similarly with respect to NH_3 desorption. Unmodified TiO_2 exhibited a broad NH_3 desorption profile ranging from 50–450 °C for FSS_Ti and 50–500 °C for WI_Ti. The NH_3-TPD profile of WI_Ti is intentionally not shown to its full scale in Fig. 5a to give a clearer picture of the NH_3-TPD profiles of the other materials and to better represent the effect of cerium and tungsten on NH_3 adsorption. The NH_3 uptake of WI_Ti was the largest among the investigated materials (Table 1), which produces the very intense and broad NH_3-TPD profile of Fig. 5a. The high content of SO_3 (~1.25 wt%) in the sample increases significantly its surface acidity. The temperature range 50–125 °C of the NH_3-TPD profiles of Fig. 5 (zone I) can be assigned to desorption of physisorbed NH_3. The temperature range 125–350 °C (zone II) is the most relevant for the SCR performance and is assigned to weak acid sites. NH_3 desorption above 350 °C (zone III) can be assigned to strong acid sites and strong surface bonding of NH_3 species that can be detrimental for the SCR performance. WO_3 suppressed the high temperature acid sites of WI_Ti that are responsible for strong NH_3 adsorption. In case of FSS, WO_3 increased the fraction of weak acid sites, thus increasing the NH_3 uptake. Ceria decreased the overall amount of weak and strong acid sites and suppressed the high temperature NH_3 desorption. As a result of the contrasting effect of WO_3 and CeO_2, the NH_3 uptake of the ternary W/Ce/Ti catalysts was intermediate between that of the binary compositions irrespective of the synthesis method.

It should be noted in Table 1 that wet-impregnated samples possess higher WO_3 coverage per unit surface area than the flame-made counterparts. The observed differences of NH_3 uptake and desorption of wet-impregnated and flame-made catalysts could be explained based on WO_3 surface coverage. Though the content of WO_3 is equal to 10 wt% on all catalysts, the specific surface area of the wet-impregnated samples is nearly 40% lower than that of their flame-made counterparts (Table 1). Therefore, the WO_3 coverage is higher for the WI-made (around 1 monolayer) than for the FSS-made (0.65 of monolayer) catalysts. Tungsten coverages below the monolayer (3–4 W atoms·nm^{-2}) are characterized by the presence of polytungstate species and mixed Lewis and Brønsted acidity.[14] Such extent of WO_x surface coverage was reported to be optimal for the NO_x reduction efficiency[15] and hydrothermal stability.[16] The flame-made catalysts exhibit WO_3 coverage in this range and thus high $DeNO_x$ activity. On the contrary, the higher tungsten coverage of the wet-impregnated catalysts generates crystalline WO_3 nanoparticles on the amorphous tungstate layer[9] and decreases the Lewis acidity.[10a] Additionally, less redox active sites are available because they are covered by the WO_3 species. Hence, the $DeNO_x$ activity of WI_W/Ce/Ti is reduced compared to that of FSS_W/Ce/Ti (Fig. 3).

Although the materials obtained by wet impregnation were produced with the aim to mimic the structure of the flame-made catalyst, clear structural and thus activity differences have been observed. The structural dissimilarities can be explained considering the different synthesis procedures. Wet impregnation is a stepwise process where TiO_2 was first impregnated with the cerium precursor and calcined, followed

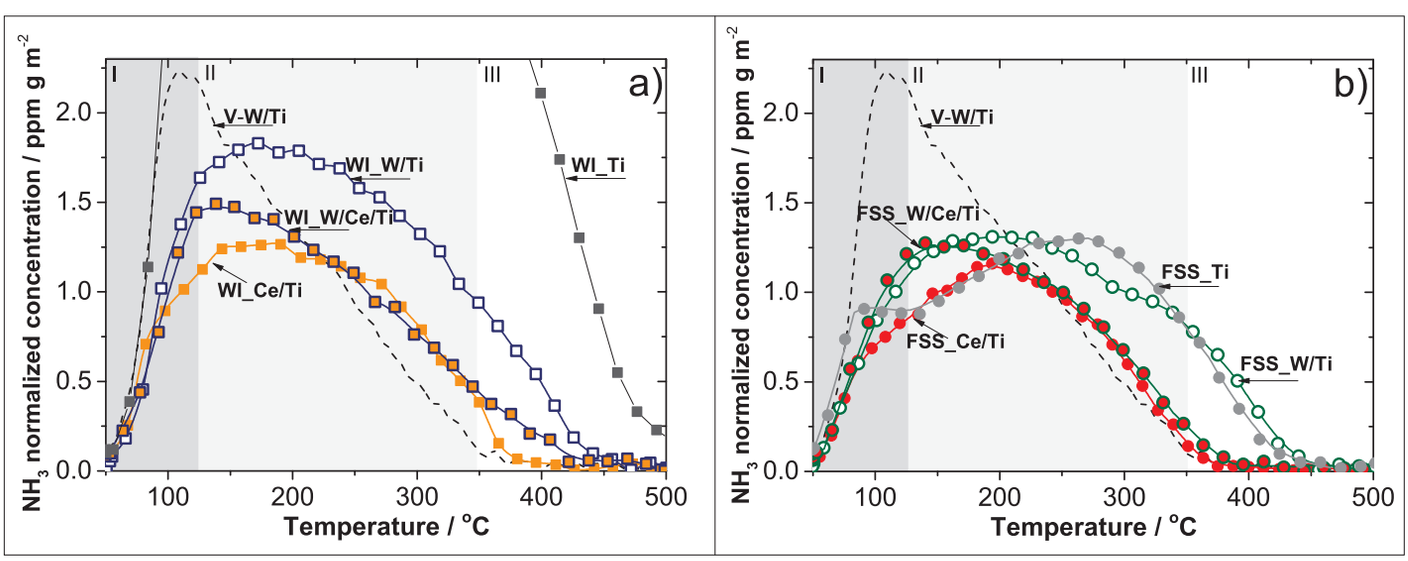

Fig. 5 NH_3-TPD profiles of wet-impregnated (a) and flame-made (b) catalysts. The dash profile corresponds to NH_3-TPD of the reference V-W/Ti catalyst. All profiles are normalized by the specific surface area of the catalyst.

by addition of the W precursor and calcination to generate supported WO_3. In flame spray synthesis, the well-mixed precursor solution of all components was sprayed into the oxygen-acetylene flame and was instantly vaporized. During particle formation, CeO_2–TiO_2 and TiO_2 particles nucleate first due to their high melting point followed by subsequent WO_3 condensation on their surface and fast quenching. The volatility of WO_3 in the high temperature zone of the flame is induced by the presence of H_2O, largely available in the flame itself as a combustion product.[17] Therefore, contrary to the classic synthesis route of an active SCR catalyst resulting in the deposition of the redox active species on WO_3/TiO_2, FSS produces a sort of 'inverse catalyst' that is characterized by strong interaction between its components that is not easily reproduced by wet impregnation. The lower $DeNO_x$ activity of WI_W/Ce/Ti can be explained by the limited interaction between the oxide components, the higher WO_3 coverage, which could block $Ce^{3+/}$ Ce^{4+}-related redox active sites, the strong NH_3 adsorption and the lower SSA.

Conclusions

Ternary 10 wt% WO_3/10 mol% CeO_2/90 mol% TiO_2 was prepared by consecutive wet impregnation of TiO_2 by the Ce and the W precursors and by one-pot flame spray synthesis. Flame-spray synthesis produces a superior active SCR catalyst whose peculiar structure cannot be mimicked using a conventional synthesis method such as wet impregnation. This is ascribed to the particular conditions of FSS. Wet impregnation is not able to reproduce the arrangement and the type of interaction between the various components that appear crucial to impart defined structural characteristics and high catalytic activity.

Received: February 3, 2015

[1] a) S. Roy, M. S. Hegde, G. Madras, *Appl. Energ.* **2009**, *86*, 2283; b) D. L. Mauzerall, B, Sultan, N. Kim, D. F. Bradford, *Atmos. Environ.* **2005**, *39*, 2851; c) H. Bosch, F. Janssen, *Catal. Today* **1988**, *2*, 369.

[2] T. V. Johnson, in 'Urea-SCR Technology for $deNO_x$ After Treatment of Diesel Exhausts', Eds. I. Nova, E. Tronconi, Springer New York, **2014**, p 3.

[3] G. Busca, L. Lietti, G. Ramis, F. Berti, *Appl. Catal. B-Environ.* **1998**, *18*, 1.

[4] X. Du, X. Gao,W. Hu, J. Yu, Z. Luo, K. Cen, *J. Phys Chem. C* **2014**, *118*, 13617.

[5] L. Zhang, J. Pierce, V. L. Leung, D. Wang, W. S. Epling, *J. Phys. Chem. C* **2013**, *117*, 8282.

[6] a) L. Chen, J. Li, M. Ge, *Environ. Sci. Technol.* **2010**, *44*, 9590; b) L. Chen, J. Li, M. Ge, R. Zhu, *Catal. Today* **2010**, *153* 77; c) W. Xu, Y. Yu, C. Zhang, H. He, *Catal. Commun.* **2008**, *9*, 1453.

[7] a) X. Gao, Y. Jiang, Y. Zhong, Z. Luo, K. Cen, *J. Hazard. Mater.* **2010**, *174*, 734; b) L. Chen, D. Weng, Z. Si, X. Wu, *Prog. Nat. Sci.* **2012**, *22*, 265.

[8] a) P. Li, Y. Xin, Q. Li, Z. Wang, Z. Zhang, L. Zheng, *Environ. Sci.Technol.* **2012**, *46*, 9600; b) W. Shan, F. Liu, H. He, X. Shi, C. Zhang, *ChemCatChem* **2011**, *3*, 1286; c) W. Shan, F. Liu, H. He, X. Shi, C. Zhang, *Appl. Catal. B-Environ.* **2012**, *115*, 100.

[9] a) C. Chaisuk, A. Wehatoranawee, S. Preampiyawat, S. Netiphat, A. Shotipruk, O. Mekasuwandumrong, *Ceram. Int.* **2011**, *37*, 1459; b) K. A. Michalow-Mauke, Y. Lu, K. Kowalski, T. Graule, O. Kröcher, *ACS Cataysis* **2015**, submitted.

[10] a) K. K. Akurati, A. Vital, J. P. Dellemann, K. Michalow, T. Graule, D. Ferri, A. Baiker, *Appl. Catal. B-Environ.* **2008**, *79*, 53; b) K. A. Michalow, A. Vital, A. Heel, T. Graule, F. A. Reifler, A. Ritter, K. Zakrzewska, M. Rekas, *J. Adv. Oxid. Technol.* **2008**, *11*, 56.

[11] M. Wojdyr, *J. Appl. Crystallogr.* **2010**, *43*, 1126.

[12] a) K. A. Michalow, E. H. Otal, D. Burnat, G. Fortunato, H. Emerich, D. Ferri, A. Heel, T. Graule, *Catal. Today* **2013**, *209*, 47; b) R. D. Shannon, J. R. Pask, *J. Am. Ceram. Soc.* **1965**, *48*, 391.

[13] J. Engweiler, J. Harf, A. Baiker, *J. Catal.* **1996**, *159*, 259.

[14] I. E. Wachs, T. Kim, E. I. Ross, *Catal. Today* **2006**, *116*, 162.

[15] L. J. Alemany, L. Lietti, N. Ferlazzo, P. Forzatti, G. Busca, E. Giamello, F. Bregani, *J. Catal.* **1995**, *155*, 117.

[16] D. M. Chapman, *Appl. Catal A-Gen.* **2011**, *392*, 143.

[17] T. Millner, J. Neugebauer, *Nature* **1949**, *163*, 601.